OPEN ACCESS
Journal of Multidisciplinary Applied Natural Science Vol. 6 No. 1 (2026) https://doi.org/10.47352/jmans.2774-3047.332
Check for updates
Research Article

Adsorption Study of Protein onto Gallic Acid Modified Fe_3O_4 Nanoparticles

Hans Kristianto, Christ Joseph Carlo Wibowo Apoenx, Stephanie Hanafi, Susiana Prasetyo, Asaf K Sugih, Wibawa Hendra Saputera, and Johnner P Sitompul*

Received : July 3, 2025	Revised : September 23, 2025	Accepted : October 29, 2025	Online : December 26, 2025

Abstract
In recent years, Fe_3O_4 nanoparticles have been widely developed as adsorbents for various applications. However, their hydrophobic surface limits their application in polar systems, necessitating surface modifications to enhance adsorption. In this study, gallic acid was employed to modify Fe_3O_4 nanoparticles, as its carboxyl and phenolic hydroxyl groups can provide sites for protein adsorption. The research aims to determine the optimal pH, adsorption capacity, isotherm models, and thermodynamic parameters for bovine serum albumin (BSA) adsorption, as a model protein, onto gallic acid-modified and unmodified Fe_3O_4 nanoparticles using batch experiments. The experiments varied pH (3.6–5.6), initial BSA concentrations (0.50–1.75 mg/L), and temperatures (30–50 °C). FTIR analysis confirmed successful modification through the presence of C=O stretching bonds, while BSA adsorption was indicated by the appearance of amide groups and transmission electron microscopy (TEM) observations. Maximum adsorption was achieved at pH 4.8, in the vicinity of BSA isoelectric point. The Langmuir isotherm model best described the adsorption process for all adsorbents. Thermodynamic analysis showed that BSA adsorption was spontaneous and endothermic with increased randomness, as evidenced by negative Gibbs free energy, along with positive enthalpy and entropy values. Surface modification with gallic acid enhanced BSA adsorption capacity to 68.49 mg/g compared to 34.84 mg/g for unmodified Fe_3O_4 at 50 °C.

Keywords: adsorption, bovine serum albumin (BSA), gallic acid, iron oxide nanoparticles, magnetite

1. INTRODUCTION

In recent years, the study of nanoparticles (ranging in size from 1 to 100 nm) has drawn significant attention from researchers across various scientific disciplines. Among various nanoparticles, iron oxide nanoparticles, especially Fe_3O_4 (magnetite), have been developed and studied due to their unique and advantageous properties, namely: being highly biocompatible, exhibiting good magnetic properties and being low in toxicity. Additionally, their reactive surface facilitates easy surface modification, making them highly versatile for a wide array of applications [1]. Fe_3O_4 nanoparticles find applications in numerous fields, including biomedicine, biosensing, energy storage, and environmental science [2]. Within the biomedical domain, they are explored for drug delivery [3], magnetic resonance imaging contrast agents, and hyperthermia treatments for cancer [4]. In the field of biosensing, Fe_3O_4 nanoparticles serve as key components in the development of sensitive and specific sensors for the detection of biomolecules [5]. In energy storage, they contribute to the development of high-performance batteries and supercapacitors [6]. Moreover, their environmental applications include water-wastewater treatment, where they have been employed as Fenton-like catalysts [7], magnetic coagulant [8]-[11], as well as for the adsorption of heavy metals, dyes, and other pollutants [12].

Given the wide range of potential applications, the study of Fe_3O_4 and protein composite synthesis through protein adsorption and immobilization has gained significant prominence. Within the scope of the aforementioned applications, the study of Fe_3O_4 and protein composite synthesis via protein adsorption/immobilization is gaining prominence. The composite of protein and nanoparticles has been widely used for various applications, such as: antibiotics adsorption [13], biosensor [14], surface imprinting [15], enzyme immobilization [16][17], natural coagulant [18], and medium for drug delivery [19][20]. To achieve a good adsorption of protein on Fe_3O_4, surface modification is used to improve the adsorption capacity. Previous studies have reported enhanced protein adsorption on Fe_3O_4

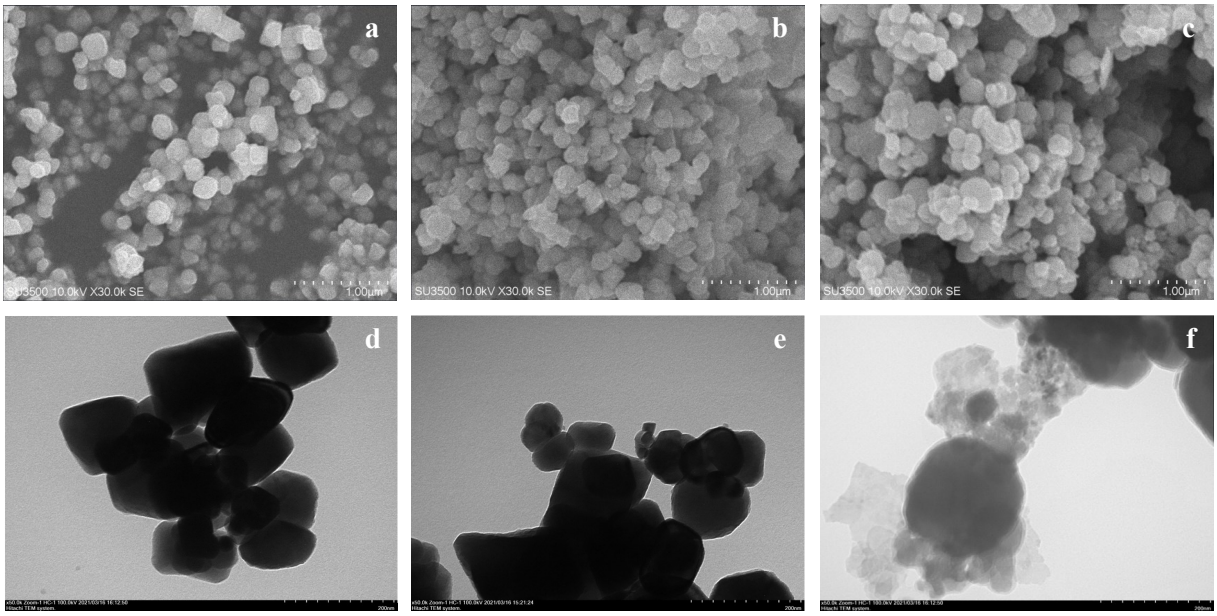

Figure 1. SEM images of (a) Fe_3O_4, (b) Fe_3O_4-BSA, and (c) Fe_3O_4-GA-BSA; and TEM images of (d) Fe_3O_4, (e) Fe_3O_4-BSA, and (f) Fe_3O_4-GA-BSA (arrows indicate the protein layer on the nanoparticle surface).

through modifications with chitosan [21], ionic liquid [15], and acids [22], resulting in adsorption capacities ranging from 36.8 to 96.6 mg/g. Among these methods, acid modification of Fe_3O_4 nanoparticles has been widely explored due to its simplicity and effectiveness. Various acids, including citric acid [22][23], oxalic acid, succinic acid, and glutamic acid [24] have been used to modify Fe_3O_4 for several applications such as cancer drug delivery and magnetic coagulant. Tannic acid has been utilized for enzyme immobilization on Fe_3O_4 nanoparticles, showcasing its potential in biocatalysis and other biotechnological applications [16][17][25].

In the present study, the use of gallic acid was investigated to modify Fe_3O_4 nanoparticles for bovine serum albumin (BSA) as a model protein substance. Gallic acid is a polyphenol that is commonly found in plants, both in free state or as a part of a complex structure. Its role as antibacterial, antifungal, antiviral, anti-inflammatory agent, as well as its high antioxidant activity has been reported in previous studies [26][27]. Gallic acid contains a carboxyl group and three phenolic hydroxyl groups that can anchor onto the Fe_3O_4 surface, thereby providing more functional sites for protein interaction, while also reducing nanoparticle agglomeration and enhancing hydrophilicity [28]. Furthermore, compared to tannic acid, the smaller gallic acid molecule provides more homogenous surface coverage and less steric hindrance, unlike the bulkier structure of tannic acid. Previous studies have demonstrated the use of gallic acid modified Fe_3O_4 in diverse applications, such as adsorption, enzyme immobilization, drug delivery, antioxidant, and antimicrobial agents [28][29][30]. Atacan et al. [29] have reported the use of gallic acid-modified Fe_3O_4 for immobilization of trypsin for hydrolysis of bovine milk. The immobilized enzyme exhibited high performance and retained stability after eight reuse cycles. Similarly, a study by Mu et al. [31] reported the use of a combination of BSA, gallic acid, and iron nanoparticles as theranostic agents with high biocompatibility.

However, despite the extensive research on gallic acid-modified Fe_3O_4 nanoparticles, there has been limited investigation into the isotherm and thermodynamics of protein adsorption Therefore, the aim of this study was to investigate the effect of various variables, namely the solution's pH, BSA concentration, and adsorption temperature on the BSA adsorption onto modified Fe_3O_4 nanoparticles compared to unmodified one. By analyzing the adsorption data, we applied several isotherm adsorption models were applied, namely the Langmuir, Freundlich, Temkin, and Dubinin-

Radushkevich (DR) models to better understand the adsorption phenomena of BSA. Additionally, the thermodynamic nature of the adsorption process was investigated, providing insights into the feasibility and spontaneity of the adsorption under different conditions. The results of this study contribute to the broader understanding of protein adsorption on Fe_3O_4 nanoparticles and pave the way for future applications of Fe_3O_4-protein composite in biomedicine, environmental science, and other fields where nanoparticle-protein composites play a crucial role.

2. MATERIALS AND METHODS

2.1. Materials

In this study, Fe_3O_4 nanoparticles (Sigma Aldrich, nanopowder < 50 nm, >97%), gallic acid (Merck, anhydrous, ≥ 98.0%), BSA (Merck, ≥ 96.0%), acetic acid (Merck, glacial, ≥ 99.0%), sodium acetate (Merck, ≥ 99.0%), and ethanol (technical grade, 96% v/v) were purchased from local suppliers and used without further purification. Demineralized water was employed for all solution preparations and experimental procedures.

2.2. Modification of Fe_3O_4

The modification of Fe_3O_4 followed the procedure outlined by Atacan and Özacar [16]. Specifically, 3.5 g of Fe_3O_4 was dispersed into 60 mL of demineralized water and sonicated for 15 min (Elma Ultrasonics PH60), followed by mixing at 200 rpm 40 °C for 1 h. Meanwhile, 2.5 g of gallic acid was dissolved into 40 mL demineralized water in a separate beaker. This solution was subsequently added to the Fe_3O_4 suspension and mixed at 200 rpm, with temperature of 40 °C for 2 h. After completion, the solid was separated using an external magnet and washed with 50 mL demineralized water, followed by 20 mL ethanol, before being dried in an oven at 60 °C for 24 h. This modified Fe_3O_4 was then stored in a desiccator for the adsorption study. The gallic acid modified Fe_3O_4 is denoted as Fe_3O_4-GA.

2.3. BSA Adsorption Study

The BSA adsorption study was conducted using the methodology outlined in our previous study [32]. Prior to the adsorption at various BSA concentrations, the best pH for the BSA adsorption was studied. Approximately 80 mg of Fe_3O_4 was added to 5 mL of a 1 mg/L BSA solution with initial pH values adjusted between 3.6 to 5.6 using an acetate buffer solution and measured using a calibrated pH meter (Hanna Instruments HI8424). The suspension was ultrasonicated for 1 min, followed by mixing at 30 °C for 4 h in a water bath shaker (Jeio Tech BS-06). After the adsorption, the Fe_3O_4 was separated using external magnet, washed using acetate buffer and oven-dried (70 °C for 12 h). The Bradford method was employed to quantify the BSA concentration [33]. The absorbance of the protein – Bradford reagent complex was measured

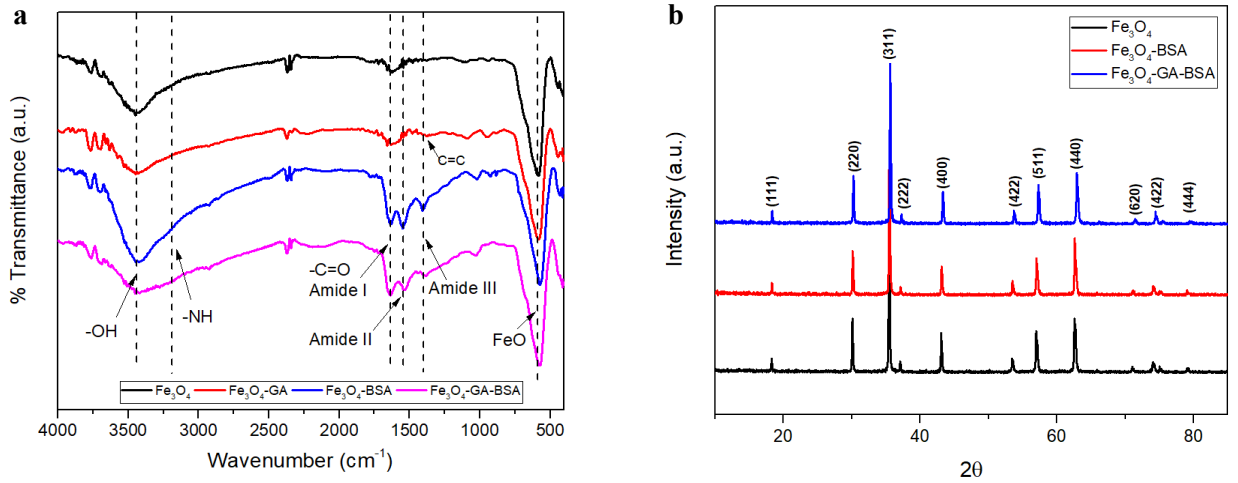

Figure 2. (a) FTIR spectra of Fe_3O_4 before and after gallic acid modification and BSA adsorption; and (b) XRD patterns of Fe_3O_4, Fe_3O_4-BSA, and Fe_3O_4-GA-BSA.

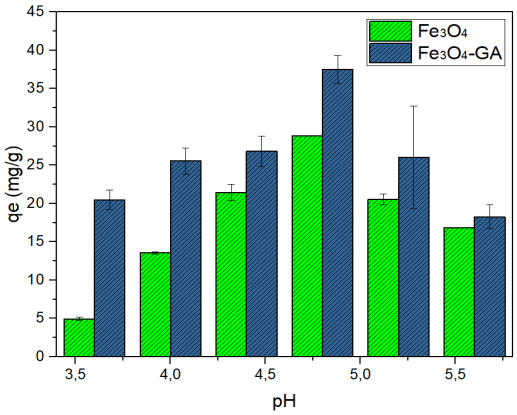

Figure 3. Effect of pH on BSA adsorption onto pristine Fe_3O_4 and Fe_3O_4-GA.

Table 1. Analysis of variance for pH variation on BSA adsorption.

Source	Sum of Squares	df	Mean Square	F	Sig.	Partial eta Squared
Corrected model	1489.158[a]	11	135.378	26.831	0.000	0.961
Intercept	11342.715	1	11342.715	2248.020	0.000	0.995
pH	967.278	5	193.456	38.341	0.000	0.941
Modif	391.731	1	391.731	77.637	0.000	0.866
pH * Modif	130.149	5	26.030	5.159	0.009	0.682
Error	60.548	12	5.046			
Total	12892.420	24				
Corrected Total	1549.705	23				

(a) R squared = 0.961 (adjusted R squared = 0.925); Modif = modification

using a spectrophotometer (Thermo Scientific Genesys 150). For isotherm adsorption and thermodynamics study, the adsorption was applied at the best pH from the previous step. Various initial BSA concentrations (0.5 to 1.75 mg/L) and adsorption temperatures (30, 40, and 50 °C) were used. All the adsorption experiments were carried out by using Fe_3O_4 and Fe_3O_4-GA as adsorbents, with two replicates for each experiment. The analysis of variance was made by using SPSS version 20.0.

2.4. Material Characterization

Following BSA adsorption, the samples were designated as Fe_3O_4-BSA and Fe_3O_4-GA-BSA, corresponding to pristine and gallic acid-modified Fe_3O_4, respectively. Material characterization was performed on both samples obtained at BSA concentration of 1.75 mg/mL and an adsorption temperature of 50 °C, which yielded the highest BSA adsorption capacity. Confirmation of successful modification and BSA adsorption was conducted using Fourier-transform infrared spectroscopy (FTIR, Prestidge 21 Shimadzu Instruments) with the KBr pellet method. The morphology of Fe_3O_4 before and after BSA adsorption was examined using a scanning electron microscope (SEM, Hitachi SU3500) and transmission electron microscope (TEM, Hitachi HT7700). X-ray diffraction (XRD, Bruker D8 Advance) was employed to analyze the crystallinity of the materials. The crystallite size (d, in nm) was estimated from the XRD patterns using the Scherrer equation (Equation (1)), where θ is the Bragg angle, K is the Scherrer constant (0.9), λ is the wavelength of Cu Kα radiation (0.15405 nm) and β is the full width at half maximum (FWHM) of the diffraction peak.

$$d = \frac{K\,\lambda}{\beta\,cos\theta} \quad (1)$$

2.5. Isotherm Adsorption Models

The adsorption capacity was calculated by using Equation (2), where qe (mg/g) is the equilibrium

adsorption capacity, Ci and Ce (mg/L) are the initial and final BSA concentration, V represents the solution's volume (L), and m denotes the mass of Fe_3O_4 or Fe_3O_4-GA (g). The adsorption capacity at various adsorption conditions was subsequently studied to determine the suitable isotherm adsorption models. The aptness of the experimental data and isotherm adsorption models was determined by the χ^2 value, which is calculated using Equation (3).

$$qe = \frac{(Ci - Ce)}{m} \times V \quad (2)$$

$$\chi^2 = \sum \frac{(qe_{experiment} - qe_{model})^2}{qe_{model}} \quad (3)$$

2.6. Adsorption Thermodynamics

The thermodynamic parameters of BSA adsorption, including Gibbs free energy (ΔG°), enthalpy (ΔH°), and entropy (ΔS°) were determined by using Equations (4) and (5). In these calculations, R represents the universal gas constant (8.314 J/mol K), while T denotes the adsorption temperature (K). The equilibrium constant (K°) was derived from the isotherm adsorption constant (K_L). This value is converted into a dimensionless K° value by using Equation (6) [34][35].

$$\Delta G° = -RTln\,(K°) \quad (4)$$

$$ln\,(K°) = \frac{-\Delta H°}{R}\frac{1}{T} + \frac{\Delta S°}{R} \quad (5)$$

$$K° = K_L\left(\frac{L}{mg}\right) \times 1000\frac{mg}{g} \times 55.51\frac{mol}{L} \times Mr\ BSA\ (\frac{g}{mol}) \quad (6)$$

3. RESULTS AND DISCUSSIONS

3.1. Characterization of Fe_3O_4 after Modification and BSA Adsorption

The morphology of pristine Fe_3O_4, Fe_3O_4-BSA, Fe_3O_4-GA-BSA was observed using SEM and TEM analyses, as shown in Figure 1. SEM images

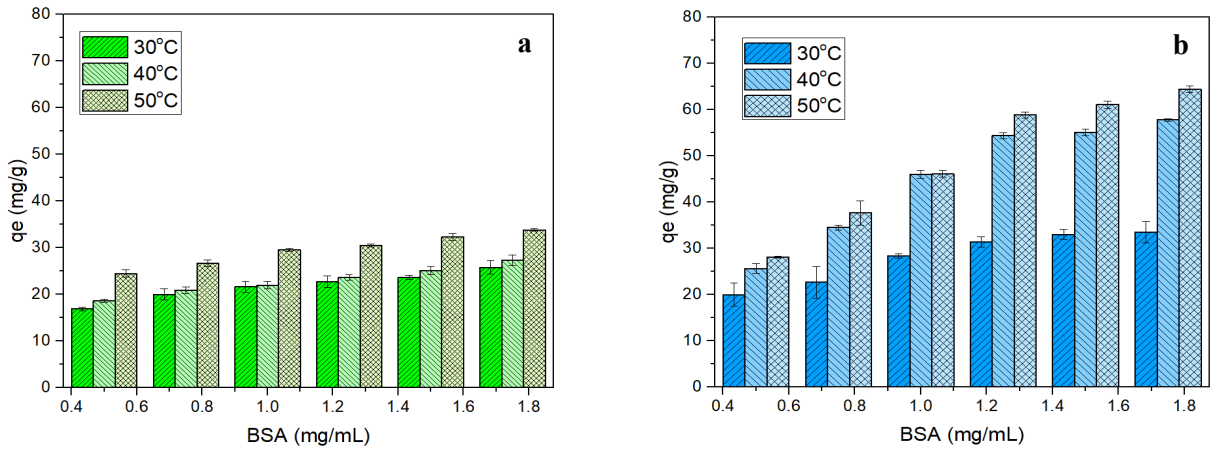

Figure 4. Adsorption capacity of BSA at various initial concentrations and temperatures on (a) Fe_3O_4 and (b) Fe_3O_4-GA.

Table 2. Analysis of variance for BSA adsorption.

Source	Sum of Squares	df	Mean Square	F	p Value
Corrected model	12692.582[a]	35	362.645	258.728	0.000
Intercept	77881.239	1	77881.239	55564.166	0.000
Modif	4784.197	1	4784.197	3413.273	0.000
Temp	2587.601	2	1293.800	923.058	0.000
Conc	3000.279	5	600.056	428.108	0.000
Modif * Temp	904.369	2	452.185	322.610	0.000
Modif * Conc	944.681	5	188.936	134.796	0.000
Temp * Conc	244.463	10	24.446	17.441	0.000
Modif * Temp * Conc	226.992	10	22.699	16.195	0.000
Error	50.459	36	1.402		
Total	90624.280	72			
Corrected total	12743.041	71			

R squared = 0.996 (adjusted R squared = .992); modif = modification, temp = temperature, conc = concentration.

Table 3. Equations and linearized forms of the isotherm models used in this study [44].

Isotherm Model	Equation	Linearized Form
Langmuir	$qe = \frac{K_L.qm.Ce}{1+K_L.Ce}$ $R_L = \frac{1}{1+K_L Ci}$	$\frac{Ce}{qe} = \frac{Ce}{qm} + \frac{1}{K_L.qm}$
Freundlich	$qe = Kf.Ce^{\frac{1}{n}}$	$log\,(qe) = log\,(K_F) + \frac{1}{n}.log\,(Ce)$
Temkin	$qe = \beta.ln\,(\alpha.Ce)$	$qe = \beta.ln\,(\alpha) + \beta.ln\,(Ce)$
Dubinin-Radushkevich	$qe = qs.e^{-\beta\varepsilon^2}$ $\varepsilon = RTln(1+\frac{1}{Ce})$	$ln\,(qe) = ln\,(qs) - \beta\varepsilon^2$

(Figures 1(a)–1(c)) revealed that Fe_3O_4 particles generally appeared as agglomerated spherical particles. Modification and BSA adsorption generally did not significantly alter the overall morphology. However, in the Fe_3O_4-BSA and Fe_3O_4-GA-BSA samples, larger agglomerates were observed compared to pristine Fe_3O_4, likely due to the presence of proteins that enhanced interparticle interactions. Further TEM analysis (Figures 1(d)–1(f)) confirmed that Fe_3O_4 particles were spherical with a tendency to agglomerate. In the Fe_3O_4-GA-BSA sample (Figure 1(f)), a grayish layer was observed on the iron nanoparticles (indicated by the arrow). This layer indicates the presence of organic compounds, specifically proteins, adsorbed onto the iron nanoparticles surface. Such a layer was not clearly visible in Fe_3O_4-BSA (Figure 1(e)), which may be attributed to the relatively lower amount of protein adsorption.

The FTIR analysis (Figure 2(a)) confirmed the successful modification using gallic acid and BSA adsorption on the Fe_3O_4. As shown in Figure 2(a), the Fe_3O_4 samples exhibited several notable peaks, specifically at 3429 and 1622 cm^{-1} corresponding to the O–H vibrational stretching of water molecules incorporated in the Fe_3O_4 framework. Additionally, a peak at 596 cm^{-1} was observed, attributed to the Fe–O vibrational mode [36]. After gallic acid modification, sharper peaks at 3429 and 1622 cm^{-1}, indicative of the O–H and C=O functional groups respectively, were observed. A broad peak at 1400 cm^{-1} was also observed that indicated the C=C bond of the gallic acid aromatic ring [37]. These changes in the FTIR spectra indicated a successful modification of Fe_3O_4 using gallic acid. After BSA adsorption, some notable peaks were observed around 1600–1700, 1500–1600, and 1200–1400 cm^{-1} corresponding to the amide I, amide II, and amide III in the structure, respectively [38]. An overlapping peak was also observed around 3200 cm^{-1} due to the N–H stretching of the protein. Furthermore, a slight peak shift was observed around Fe–O which may indicate the bonding of gallic acid and BSA on the Fe_3O_4 surface. Another minor shift was also observed for the amide II and III peaks in Fe_3O_4-GA-BSA compared to Fe_3O_4-BSA suggesting the interactions between BSA and gallic acid.

The crystallinity of the samples was measured by XRD, as shown in Figure 2(b). The diffraction peaks were identified at 18.3° (111), 30.1° (202), 35.5° (311), 37.1° (222), 43.1° (400), 53.5° (422), 57° (511), 62.6° (440), 71.4° (620), 74.1° (533), and 79° (444) corresponding to Fe_3O_4 (JCPDS 19-629) [39]. The XRD spectra indicate that there were no significant changes of the Fe_3O_4 crystal structure after gallic acid modification and BSA adsorption. Using the Scherrer equation, the crystallite sizes were calculated as 35.83, 38.43, and 37.93 nm for Fe_3O_4, Fe_3O_4-BSA, and Fe_3O_4-GA-BSA, respectively. These results confirm the nanoscale nature of the materials, and the similar crystallite sizes further validate that the crystal structure remained unchanged after modification and protein adsorption.

3.2. The Effect of pH on BSA Adsorption

Figure 3 illustrates the impact of pH on BSA adsorption. Generally, it can be seen that with the increase of pH from 3.6 to 4.8, the adsorption capacity of BSA increased. After pH 4.8, the adsorption capacity decreased. Similar results have

Table 4. Isotherm model parameters for BSA adsorption onto Fe_3O_4 and Fe_3O_4-GA at different temperatures.

Model	Parameters	Fe_3O_4			Fe_3O_4-GA		
		30 °C	**40 °C**	**50 °C**	**30 °C**	**40 °C**	**50 °C**
Langmuir	K_L (L/mg)	5.574	7.682	17.938	6.024	23.143	36.500
	qm (mg/g)	29.412	29.586	34.843	39.526	61.728	68.493
	R_L	0.092–0.264	0.069–0.206	0.030–0.100	0.086–0.249	0.024–0.079	0.015–0.051
	χ^2	0.121	0.455	4.248	0.908	0.640	5.550
Freundlich	1/n	0.260	0.196	0.110	0.284	0.269	0.256
	Kf	25.340	26.266	33.090	34.930	72.194	90.448
	χ^2	0.042	0.066	0.209	0.476	1.252	3.299
Temkin	β (J/mol)	5.413	4.399	3.139	7.455	10.836	11.162
	α (L/mg)	103.519	381.764	36103.240	99.705	430.827	1050.004
	χ^2	0.047	0.101	0.262	0.532	0.572	2.446
Dubinin-Radushkevich	K (mol^2/J^2)	0.0027	0.0012	8×10^{-5}	0.0012	8×10^{-5}	1×10^{-5}
	qs (mg/g)	23.9507	24.5816	30.0481	30.7134	50.8917	53.4902
	χ^2	0.3663	0.6354	1.0071	1.8696	4.2349	8.7713

been reported by previous studies [32][40]. It is known that the highest BSA adsorption occurred near its isoelectric point (pI) of 4.5–4.8 [41]. At its pI, the conformational shift of BSA structure makes the BSA structure compact, which reduces the repulsive force between BSA and the adsorbent. At the pH above BSA pI, the adsorption capacity decreased due to the expansion of the BSA structure, hindering the interaction of BSA-adsorbent [42]. The analysis of variance for the effects of modification and pH to BSA adsorption is presented in Table 1. It can be observed that pH, modification, and their interaction significantly affected the BSA adsorption capacity (p-value < 0.05). Furthermore, the least significant difference (LSD) analysis (Table S1) showed that the pH 4.8 was significantly different from the other pH values. Therefore, pH 4.8 was subsequently employed in the investigation of adsorption isotherms.

3.3. The Influence of Concentration and Temperature on BSA Adsorption

Figure 4 illustrates the dependence of adsorption capacity on BSA concentration and adsorption temperature. Noticeably, increased initial BSA concentration resulted in more BSA adsorbed on the adsorbent. With more BSA molecules present in the solution, more effective interaction of adsorbate -adsorbent occurred, resulting in more protein being adsorbed [43]. The influence of adsorption temperature exhibited similar trend. The higher the adsorption temperature, the more BSA was adsorbed. This trend might indicate that the adsorption on both adsorbents was endothermic. Under optimal conditions of 1.75 mg/mL BSA concentration and a temperature of 50 °C, the adsorption capacity reached 34.84 mg/g for Fe_3O_4 and significantly increased to 68.49 mg/g for Fe_3O_4-GA. The analysis of variance was employed to further explore the influence of modification, BSA concentration, and temperature on the studied

Table 5. Comparison of Langmuir qm for BSA on different adsorbents.

Adsorbent	qm Langmuir (mg/g)	Temperature (°C)	Reference
Fe_3O_4-GA	68.49	50	This study
Fe_3O_4	34.84	50	This study
TiO_2	44.40	40	[46]
Hydroxyapatite	28.00	37	[47]
Kaolinite	33.02	25	[48]
Ionic liquid functionalized Fe_3O_4	36.80	25	[15]
Citrate modified Fe_3O_4	83.00	25	[22]

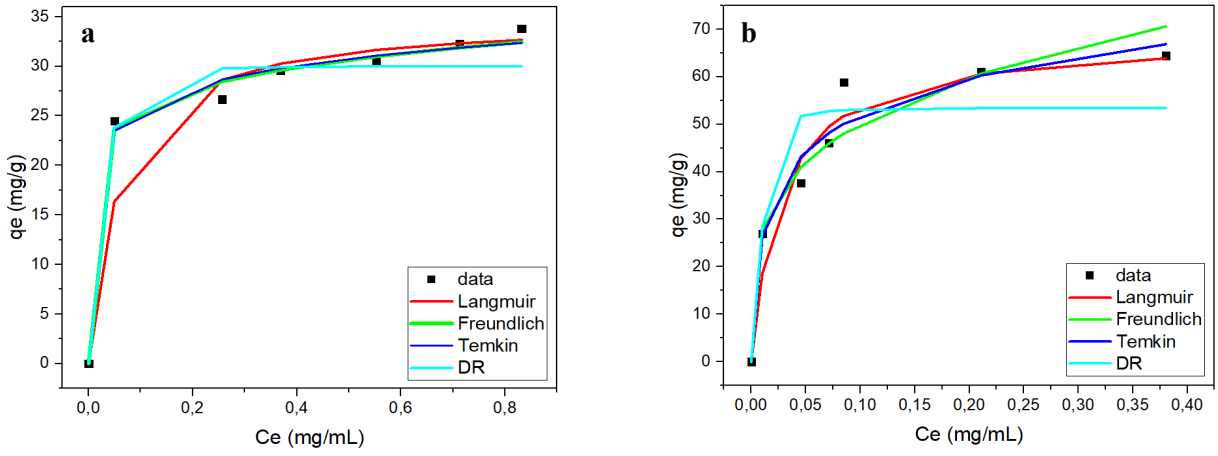

Figure 5. Fitting of experimental adsorption data to isotherm models (Langmuir, Freundlich, Temkin, and Dubinin-Radushkevich) for BSA adsorption onto (a) Fe_3O_4 and (b) Fe_3O_4-GA at 50°C.

Table 6. Thermodynamics parameter of BSA adsorption onto Fe_3O_4 and Fe_3O_4-GA at different temperatures.

T (°C)	Fe_3O_4			Fe_3O_4-GA		
	ΔG° (kJ/mol)	ΔH° (kJ/mol)	ΔS° (J/mol K)	ΔG° (kJ/mol)	ΔH° (kJ/mol)	ΔS° (J/mol K)
30	-59.85			-60.05		
40	-62.66	47.35	352.87	-65.53	73.73	442.39
50	-66.94			-68.85		

parameters, as presented in Table 2. It is evident that modification, initial BSA concentration, temperature, and their interactions are significant parameters to the adsorption capacity with confidence level of 95%, as indicated in the p values < 0.05. Furthermore, the LSD analysis (Tables S2–S3) confirmed that pairwise comparisons among all temperature and BSA concentration levels were significantly different.

3.4. Isotherm Adsorption Study

A deeper understanding of BSA adsorption on both adsorbents was sought through further isotherm study. This analysis involved the application of various isotherm models, including Langmuir, Freundlich, Temkin, and Dubinin-Radushkevich (DR). The equations for these isotherm models are provided in Table 3, while the fitting results are shown in Table 4.

The Langmuir isotherm model postulates that adsorption occurs at a single layer level on homogenous surfaces where all sites share equivalent adsorption energy. For the Langmuir model, qm is the Langmuir maximum adsorption capacity while K_L stands for the Langmuir constant. It can be seen that the modification of Fe_3O_4 and higher adsorption temperature increased the maximum adsorption capacity. This denotes the effectiveness of surface modification where gallic acid can interact with BSA molecules via hydrophobic cavities [30] as well as hydrogen bonding [45]. The positive correlation between adsorption capacity and temperature indicates the endothermic nature of the adsorption process. Observing the Langmuir separation factor (R_L), all the values lie between 0 to 1, which indicates a favorable adsorption process. Comparison of BSA adsorption in this study with the previous literature is presented in Table 5. Noticeably, the Fe_3O_4-GA gave a comparable result of BSA adsorption capacity compared to other modification methods, employing a simpler approach.

The Freundlich model, which accounts for multilayer adsorption on heterogeneous surfaces characterized by varying adsorption energies, demonstrated an increase in the Freundlich constant (Kf) with both Fe_3O_4 modification and increasing temperature. This observation suggests a positive impact of surface modification and temperature on the adsorption of BSA. Moreover, by noting that the value of 1/n, which describes the intensity of the adsorption, lies between 0 to 1 in all variations. Based on this, we can infer that the adsorption of BSA was favorable. The Temkin isotherm model posits that the heat of adsorption is a function of temperature, and the number of adsorbate molecules diminishes linearly with the increase of surface coverage of the adsorbate [49]. In the Temkin isotherm, the α value represents the maximum binding energy. The higher the temperature increases for both adsorbents, the higher α values that were obtained, confirming the endothermic nature of the adsorption [50]. The DR model, predicated on the Polanyi potential (ε) and a Gaussian distribution of adsorption energies on heterogeneous surfaces [44], demonstrated a positive correlation between temperature and maximum adsorption capacity (qs) for both adsorbents. Furthermore, the modified adsorbent exhibited a greater qs value. This finding aligns with the results from the previous isotherm adsorption models analysis. The aptness of the experimental data with the isotherm adsorption model can now be determined based on the χ^2 value and the data-model fitting (Figure 5). The Langmuir isotherm model exhibited the low chi-squared (χ^2) value, suggesting it was the best fit for the data in this study, as also shown in Figure 5. This result is

in accordance with the previously reported studies [51]-[53], that reported a monolayer nature of protein adsorption.

3.5. Adsorption Thermodynamics

Thermodynamic parameters (Table 6) revealed that BSA adsorption was a spontaneous process, as demonstrated by the negative Gibbs free energy and positive entropy values. Furthermore, the degree of spontaneity increased with higher adsorption temperatures. In addition, adsorption of BSA was endothermic, indicated by positive enthalpy value. Moreover, observing the values of enthalpy can illustrate the nature of adsorption. It is known that the physisorption process results in enthalpy below 40 kJ/mol, and chemisorption at values of 80–400 kJ/mol. The enthalpy value between ~50–70 kJ/mol might indicate a stronger bond such as hydrogen bonds [54]. ΔG° values provide a means of classifying adsorption. Values between 0 and -20 kJ/mol indicate physisorption, while values between -80 and -400 kJ/mol suggest chemisorption. The ΔG° values in this study indicate that BSA adsorption is a combination of chemisorption and physisorption [55].

Figure 6 illustrates the potential bonding mechanisms between Fe_3O_4-BSA and Fe_3O_4-GA-BSA. BSA can bind directly to Fe_3O_4 through electrostatic interactions and coordination bonds, either monodentate or bidentate [56]. In contrast, gallic acid, which is bound to Fe_3O_4 via hydrogen bonding [57], facilitates stronger protein bonds through both hydrogen and hydrophobic interactions [58]. This may be due to the presence of stronger bonds, compared to the electrostatic interactions, contributing to the increased adsorption enthalpy observed in Fe_3O_4-GA-BSA. relative to Fe_3O_4-BSA.

4. CONCLUSIONS

In this study, Fe_3O_4 nanoparticles were successfully modified using gallic acid for BSA adsorption. FTIR analysis confirmed the modification, which resulted in a substantial increase in adsorption capacity, reaching 68.49 mg/g compared to 34.84 mg/g for unmodified Fe_3O_4 at 50 °C. Furthermore, adsorption capacity was significantly influenced by surface modification, adsorption temperature, and initial BSA concentration. The Langmuir model was identified as the most appropriate, indicating monolayer adsorption of BSA. Thermodynamic analysis revealed that the adsorption of BSA onto both Fe_3O_4 and Fe_3O_4-GA was endothermic, as shown by positive enthalpy change ($\Delta H° > 0$). The process was also spontaneous, demonstrated by the negative Gibbs free energy values ($\Delta G° < 0$) and positive

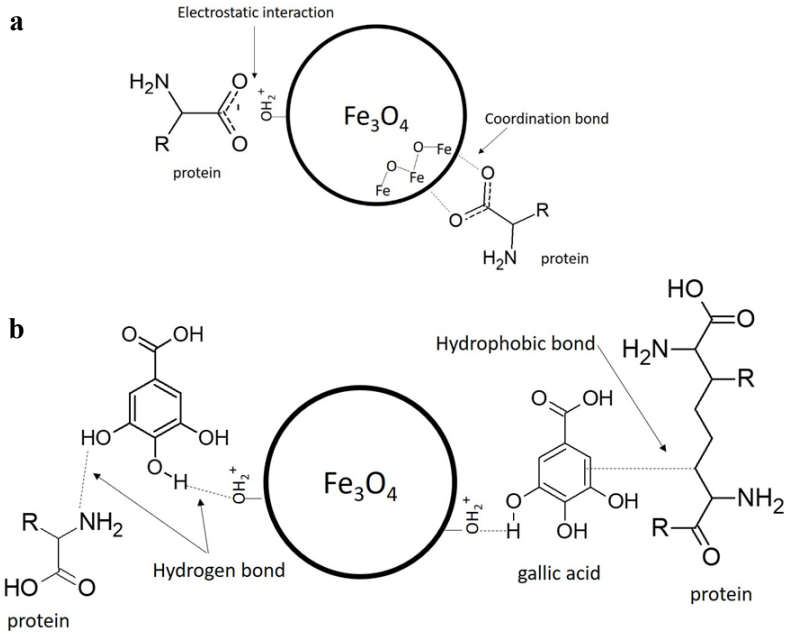

Figure 6. Schematic illustration of interactions between (a) Fe_3O_4-BSA (a) and (b) Fe_3O_4-GA-BSA.

entropy change ($\Delta S° > 0$), indicating increased randomness with surface modification and higher temperatures.

AUTHOR INFORMATION

Corresponding Author

Johnner P Sitompul — Department of Chemical Engineering, Institut Teknologi Bandung, Bandung-40132 (Indonesia);
orcid.org/0000-0003-1183-2809
Email: sitompul@itb.ac.id

Authors

Hans Kristianto — Doctoral Program of Chemical Engineering, Institut Teknologi Bandung, Bandung-40132 (Indonesia); Department of Chemical Engineering, Parahyangan Catholic University, Bandung-40141 (Indonesia);
orcid.org/0000-0003-4747-4361

Christ Joseph Carlo Wibowo Apoenx — Department of Chemical Engineering, Parahyangan Catholic University, Bandung-40141 (Indonesia);
orcid.org/0009-0008-3443-126X

Stephanie Hanafi — Department of Chemical Engineering, Parahyangan Catholic University, Bandung-40141 (Indonesia);
orcid.org/0009-0006-5298-6942

Susiana Prasetyo — Department of Chemical Engineering, Parahyangan Catholic University, Bandung-40141 (Indonesia);
orcid.org/0000-0001-5839-0054

Asaf K Sugih — Department of Chemical Engineering, Parahyangan Catholic University, Bandung-40141 (Indonesia);
orcid.org/0000-0003-0478-540X

Wibawa Hendra Saputera — Department of Chemical Engineering, Institut Teknologi Bandung, Bandung-40132 (Indonesia);
orcid.org/0000-0002-2899-0558

Author Contributions

Conceptualization, Investigation, Formal Analysis, and Writing – Original Draft: H. K.; Investigation, and Formal Analysis: C. J. C. W. A., S. H.; Methodology: S. P., A. K. S.; Writing – Review & Editing, and Supervision: W. H. S., J. P. S.; Writing – Review & Editing S. P., A. K. S., W. H. S., J. P. S.

Conflicts of Interest

The authors declare no conflict of interest.

SUPPORTING INFORMATION

Supplementary data associated with this article can be found in the online version at doi: 10.47352/jmans.2774-3047.332

ACKNOWLEDGEMENT

This research was supported by funding from the Indonesian Education Scholarship (BPI), the Center for Higher Education Funding and Assessment (PPAPT), and the Indonesia Endowment Fund for Education (LPDP).

DECLARATION OF GENERATIVE AI

Not applicable.

REFERENCES

[1] L. Shen, B. Li, and Y. Qiao. (2018). "Fe3O4 Nanoparticles in Targeted Drug/Gene Delivery Systems". *Materials.* **11** (2): 324. 10.3390/ma11020324.

[2] M. D. Nguyen, H. V. Tran, S. Xu, and T. R. Lee. (2021). "Fe3O4 Nanoparticles: Structures, Synthesis, Magnetic Properties, Surface Functionalization, and Emerging Applications". *Applied Sciences.* **11** (23): 11301. 10.3390/app112311301.

[3] E. U. Ikhuoria, I. E. Uwidia, R. O. Okojie, I. H. Ifijen, I. D. Chikaodili, and A. Fatiqin. (2024). "Advancing Green Nanotechnology: Harnessing the Bio-Reducing Properties of Musa paradisiaca Peel Extract for Sustainable Synthesis of Iron Oxide Nanoparticles". *Journal of Multidisciplinary Applied Natural Science.* **4** (1): 108-119. 10.47352/jmans.2774-3047.194.

[4] L. S. Ganapathe, M. A. Mohamed, R. M. Yunus, and D. D. Berhanuddin. (2020). "Magnetite (Fe3O4) Nanoparticles in Biomedical Applications: From Synthesis to

Surface Functionalisation". *Magnetochemistry.* **6** (4): 68. 10.3390/magnetochemistry6040068.

[5] S. E. Kim, M. V. Tieu, S. Y. Hwang, and M. H. Lee. (2020). "Magnetic Particles: Their Applications from Sample Preparation to Biosensing Platforms". *Micromachines.* **11** (3): 302. 10.3390/mi11030302.

[6] S. Yu, V. M. H. Ng, F. Wang, Z. Xiao, C. Li, L. B. Kong, W. Que, and K. Zhou. (2018). "Synthesis and Application of Iron-Based Nanomaterials as Anodes for Lithium-Ion Batteries and Supercapacitors". *Journal of Materials Chemistry A.* **6** (20): 9332-9367. 10.1039/C8TA01683F.

[7] H. Kristianto, S. Prasetyo, and A. K. Sugih. (2022). "Green-Synthesized Iron Nanoparticles Using Leucaena leucocephala Crude Extract as a Fenton-Like Catalyst". 2493 : 050001. 10.1063/5.0109914

[8] E. D. Suhardi, F. V. Hermawan, H. Kristianto, S. Prasetyo, and A. K. Sugih. (2024). "Enhancing Water–Wastewater Treatment Efficiency: A Synergistic Approach Using Polyaluminum Chloride, Sodium Alginate, and Magnetite for Congo Red Removal". *Chemical Papers.* **78** : 3971-3981. 10.1007/s11696-024-03367-9.

[9] H. Kristianto, W. H. Saputera, and J. P. Sitompul. (2025). "Novel Developments in Magnetic Coagulation: Enhancing Water and Wastewater Treatment Efficiency". *International Journal of Environmental Science and Technology.* 10.1007/s13762-025-06668-y.

[10] A. K. Sugih, M. A. Deiza, S. F. Nurmawan, S. Prasetyo, D. Tan, and H. Kristianto. (2025). "Combination of FeCl3 and Fe3O4 as a Magnetic Coagulant for Congo Red Removal". *Indonesian Journal of Urban and Environmental Technology.* **8** (1): 99-115. 10.25105/urbanenvirotech.v8i1.22575.

[11] H. Kristianto, W. H. Saputera, and J. P. Sitompul. (2025). "Small-Scale Protocol for Magnetic Coagulation Testing". *MethodsX.* **15** 103550. 10.1016/j.mex.2025.103550.

[12] Y. Shen, B. Jiang, and Y. Xing. (2021). "Recent Advances in the Application of Magnetic Fe3O4 Nanomaterials for the Removal of Emerging Contaminants". *Environmental Science and Pollution Research.* **28** : 7599-7620. 10.1007/s11356-020-11877-8.

[13] B. Zhang, H. Zhang, X. Li, X. Lei, C. Li, D. Yin, X. Fan, and Q. Zhang. (2013). "Synthesis of BSA/Fe3O4 Magnetic Composite Microspheres for Adsorption of Antibiotics". *Materials Science and Engineering C.* **33** (7): 4401-4408. 10.1016/j.msec.2013.06.038.

[14] C. He, M. Xie, F. Hong, X. Chai, H. Mi, X. Zhou, L. Fan, Q. Zhang, T. Ngai, and J. Liu. (2016). "A Highly Sensitive Glucose Biosensor Based on Gold Nanoparticles/Bovine Serum Albumin/Fe3O4 Biocomposite Nanoparticles". *Electrochimica Acta.* **222** : 1709-1715. 10.1016/j.electacta.2016.11.162.

[15] L. Qian, J. Sun, C. Hou, J. Yang, Y. Li, D. Lei, M. Yang, and S. Zhang. (2017). "Immobilization of Bovine Serum Albumin on Ionic Liquid-Functionalized Magnetic Fe3O4 Nanoparticles for Use in a Surface Imprinting Strategy". *Talanta.* **168** : 174-182. 10.1016/j.talanta.2017.03.044.

[16] K. Atacan and M. Ozacar. (2015). "Characterization and Immobilization of Trypsin on Tannic Acid-Modified Fe3O4 Nanoparticles". *Colloids and Surfaces B: Biointerfaces.* **128** : 227-236. 10.1016/j.colsurfb.2015.01.038.

[17] K. Atacan, B. Cakiroglu, and M. Ozacar. (2017). "Efficient Protein Digestion Using Immobilized Trypsin onto Tannin-Modified Fe3O4 Magnetic Nanoparticles". *Colloids and Surfaces B: Biointerfaces.* **156** : 9-18. 10.1016/j.colsurfb.2017.04.055.

[18] E. Hermawan, L. U. Carmen, H. Kristianto, S. Prasetyo, A. K. Sugih, and A. A. Arbita. (2022). "Synthesis of Magnetic Natural Coagulants and Their Application for Treating Congo Red Synthetic Wastewater". *Water, Air, and Soil Pollution.* **233** : 443. 10.1007/s11270-022-05923-z.

[19] H. Nosrati, M. Adibtabar, A. Sharafi, H. Danafar, and M. H. Kheiri. (2018). "PAMAM-Modified Citric Acid-Coated Magnetic Nanoparticles as pH-Sensitive Biocompatible Carriers Against Human

Breast Cancer Cells". *Drug Development and Industrial Pharmacy.* **44** (8): 1377-1384. 10.1080/03639045.2018.1451881.

[20] H. Nosrati, N. Sefidi, A. Sharafi, H. Danafar, and H. K. Manjili. (2018). "Bovine Serum Albumin-Coated Iron Oxide Magnetic Nanoparticles as Biocompatible Carriers for Curcumin Anticancer Drug". *Bioorganic Chemistry.* **76** : 501-509. 10.1016/j.bioorg.2017.12.033.

[21] M. Shen, Y. Yu, G. Fan, G. Chen, Y. M. Jin, W. Tang, and W. Jia. (2014). "Synthesis and Characterization of Monodispersed Chitosan-Coated Fe3O4 Nanoparticles via a Facile One-Step Solvothermal Process for Adsorption of Bovine Serum Albumin". *Nanoscale Research Letters.* **9** : 296. 10.1186/1556-276X-9-296.

[22] Z. U. Rahman, Y. Dong, C. Ren, Z. Zhang, and X. Chen. (2012). "Protein Adsorption on Citrate-Modified Magnetic Nanoparticles". *Journal of Nanoscience and Nanotechnology.* **12** : 2598-2606. 10.1166/jnn.2012.5751.

[23] H. Kristianto, E. Reynaldi, S. Prasetyo, and A. K. Sugih. (2020). "Adsorbed Leucaena Protein on Citrate-Modified Fe3O4 Nanoparticles: Synthesis, Characterization, and Application as a Magnetic Coagulant". *Sustainable Environment Research.* **30** : 32. 10.1186/s42834-020-00074-4.

[24] R. Neha, A. Jaiswal, J. Bellare, and N. K. Sahu. (2017). "Synthesis of Surface-Grafted Mesoporous Magnetic Nanoparticles for Cancer Therapy". *Journal of Nanoscience and Nanotechnology.* **17** : 5181-5188. 10.1166/jnn.2017.13853.

[25] Q. Xiao, C. Liu, H. Ni, Y. Zhu, Z. Jiang, and A. Xiao. (2019). "β-Agarase Immobilized on Tannic Acid-Modified Fe3O4 Nanoparticles for Efficient Preparation of Bioactive Neoagaro-Oligosaccharides". *Food Chemistry.* **272** : 586-595. 10.1016/j.foodchem.2018.08.017.

[26] B. Badhani, N. Sharma, and R. Kakkar. (2015). "Gallic Acid: A Versatile Antioxidant with Promising Therapeutic and Industrial Applications". *RSC Advances.* **5** : 27540-27557. 10.1039/C5RA01911G.

[27] N. A. A. Al-Zahrani, R. M. El-Shishtawy, and A. M. Asiri. (2020). "Recent Developments of Gallic Acid Derivatives and Their Hybrids in Medicinal Chemistry: A Review". *European Journal of Medicinal Chemistry.* **204** : 112609. 10.1016/j.ejmech.2020.112609.

[28] S. T. Shah, W. A. Yehya, O. Saad, K. Simarani, Z. Chowdhury, A. A. Alhadi, and L. A. Al-Ani. (2017). "Surface Functionalization of Iron Oxide Nanoparticles with Gallic Acid as Potential Antioxidant and Antimicrobial Agents". *Nanomaterials.* **7** (10): 306. 10.3390/nano7100306.

[29] K. Atacan, B. Cakiroglu, and M. Ozacar. (2016). "Improvement of Stability and Activity of Immobilized Trypsin on Modified Fe3O4 Magnetic Nanoparticles for Hydrolysis of Bovine Serum Albumin and Application in Bovine Milk". *Food Chemistry.* **212** : 460-468. 10.1016/j.foodchem.2016.06.011.

[30] D. Dorniani, M. Z. Hussein, A. U. Kura, S. Fakurazi, A. H. Shaari, and Z. Ahmad. (2012). "Preparation of Fe3O4 Magnetic Nanoparticles Coated with Gallic Acid for Drug Delivery". *International Journal of Nanomedicine.* **7** : 5745-5756. 10.2147/IJN.S35746.

[31] X. Mu, C. Yan, Q. Tian, J. Lin, and S. Yang. (2017). "BSA-Assisted Synthesis of Ultrasmall Gallic Acid–Fe(III) Coordination Polymer Nanoparticles for Cancer Theranostics". *International Journal of Nanomedicine.* **12** : 7207-7223. 10.2147/IJN.S146064.

[32] H. Kristianto, J. Alexander, S. Prasetyo, and A. K. Sugih. (2022). "Tannic Acid-Modified Iron Oxide Nanoparticles and Their Application in Protein Adsorption: Isotherm, Kinetic, and Thermodynamic Studies". *Molekul.* **17** (1): 49-59. 10.20884/1.jm.2022.17.1.5571.

[33] M. M. Bradford. (1976). "A Rapid and Sensitive Method for the Quantitation of Microgram Quantities of Protein Utilizing the Principle of Protein–Dye Binding".

Analytical Biochemistry. **72** : 248-254. 10.1016/0003-2697(76)90527-3.

[34] E. C. Lima, A. Hosseini-Bandegharaei, J. C. Moreno-Piraján, and I. Anastopoulos. (2019). "A Critical Review of the Estimation of Thermodynamic Parameters on Adsorption Equilibria: Wrong Use of Equilibrium Constants in the Van't Hoff Equation". *Journal of Molecular Liquids.* **273** : 425-434. 10.1016/j.molliq.2018.10.048.

[35] H. N. Tran, E. C. Lima, R. S. Juang, J. C. Bollinger, and H. P. Chao. (2021). "Thermodynamic Parameters of Liquid-Phase Adsorption Processes Calculated from Different Equilibrium Constants: A Comparison Study". *Journal of Environmental Chemical Engineering.* **9** (6): 106674. 10.1016/j.jece.2021.106674.

[36] N. R. Jannah and D. Onggo. (2019). "Synthesis of Fe3O4 Nanoparticles for Colour Removal of Printing Ink Solutions". *IOP Conference Series: Journal of Physics: Conference Series.* **1245** : 012040. 10.1088/1742-6596/1245/1/012040.

[37] A. R. Khaskheli, S. Naz, F. Ozul, A. Aljabour, S. A. Mahesar, I. H. Patir, and M. Ersoz. (2016). "Urchin-Like Cobalt Nanostructures for Catalytic Degradation of Nitroanilines". *Advanced Materials Letters.* **7** (9): 748-753. 10.5185/amlett.2016.6264.

[38] K. H. Sizeland, K. A. Hofman, I. C. Hallett, D. E. Martin, J. Potgieter, N. M. Kirby, A. Hawley, S. T. Mudie, T. M. Ryan, R. G. Haverkamp, and M. H. Cumming. (2018). "Nanostructure of Electrospun Collagen: Do Electrospun Collagen Fibers Form Native Structures?". *Materialia.* **3** : 90-96. 10.1016/j.mtla.2018.10.001.

[39] D. Pop, R. Buzatu, E. A. Moacă, C. G. Watz, S. C. Pînzaru, L. B. Tudoran, F. Nekvapil, Ș. Avram, C. A. Dehelean, M. O. Crețu, M. Nicolov, C. Szuhanek, and A. Jivănescu. (2021). "Development and Characterization of Fe3O4@Carbon Nanoparticles and Their Biological Screening Related to Oral Administration". *Materials.* **14** (13): 3556. 10.3390/ma14133556.

[40] M. S. C. Barreto, E. J. Elzinga, and L. R. F. Alleoni. (2020). "Molecular Insights into Protein Adsorption on Hematite Surfaces Disclosed by In Situ ATR-FTIR/2D-COS Study". *Scientific Reports.* **10** : 13441. 10.1038/s41598-020-70201-z.

[41] V. S. Raghuwanshi, B. Yu, C. Browne, and G. Garnier. (2020). "Reversible pH-Responsive Bovine Serum Albumin Hydrogel Sponge Nanolayer". *Frontiers in Bioengineering and Biotechnology.* **8** : 573. 10.3389/fbioe.2020.00573.

[42] G. R. Mahdavinia and H. Etemadi. (2019). "Surface Modification of Iron Oxide Nanoparticles with κ-Carrageenan/ Carboxymethyl Chitosan for Effective Adsorption of Bovine Serum Albumin". *Arabian Journal of Chemistry.* **12** (8): 3692-3703. 10.1016/j.arabjc.2015.12.002.

[43] C. H. Kim, Z. F. Zhang, L. S. Wang, and T. Sun. (2020). "Preparation of MnO2-Impregnated Carbon-Coated Fe3O4 Nanocomposites and Their Application for Bovine Serum Albumin Adsorption". *Rare Metals.* **39** (3): 1151-1158. 10.1007/s12598-016-0779-3.

[44] M. M. Majd, V. Kordzadeh-Kermani, V. Ghalandari, A. Askari, and M. Sillanpaa. (2022). "Adsorption Isotherm Models: A Comprehensive and Systematic Review (2010–2020)". *Science of the Total Environment.* **812** : 151334. 10.1016/j.scitotenv.2021.151334.

[45] M. Zhang, L. Fan, Y. Liu, and J. Li. (2023). "Migration of Gallic Acid from the Aqueous Phase to the Oil–Water Interface Using Pea Protein to Improve the Physicochemical Stability of Water-in-Oil Emulsions". *Food Hydrocolloids.* **135** : 108179. 10.1016/j.foodhyd.2022.108179.

[46] T. Kopac and K. Bozgeyik. (2010). "Effect of Surface Area Enhancement on the Adsorption of Bovine Serum Albumin onto Titanium Dioxide". *Colloids and Surfaces B: Biointerfaces.* **76** (1): 265-271. 10.1016/j.colsurfb.2009.11.002.

[47] S. K. Swain and D. Sarkar. (2013). "Study of Bovine Serum Albumin Protein Adsorption and Release on Hydroxyapatite Nanoparticles". *Applied Surface Science.* **286** 99-103. 10.1016/j.apsusc.2013.09.027.

[48] M. Alkan, O. Demirbas, M. Dogan, and O. Arslan. (2006). "Surface Properties of Bovine Serum Albumin-Adsorbed Oxides: Adsorption, Kinetics, and Electrokinetic Properties". *Microporous and Mesoporous Materials.* **96** (1-3): 331-340. 10.1016/j.micromeso.2006.07.007.

[49] M. A. Al-Ghouti and D. A. Daana. (2020). "Guidelines for the Use and Interpretation of Adsorption Isotherm Models: A Review". *Journal of Hazardous Materials.* **393** : 122383. 10.1016/j.jhazmat.2020.122383.

[50] A. M. Aljeboree, A. N. Alshirifi, and A. F. Alkaim. (2017). "Kinetics and Equilibrium Study for the Adsorption of Textile Dyes on Coconut Shell Activated Carbon". *Arabian Journal of Chemistry.* **10** : S3381-S3393. 10.1016/j.arabjc.2014.01.020.

[51] M. P. Schmidt and C. E. Martinez. (2016). "Kinetic and Conformational Insights of Protein Adsorption onto Montmorillonite Revealed Using In Situ ATR-FTIR/2D-COS". *Langmuir.* **32** (31): 7719-7729. 10.1021/acs.langmuir.6b00786.

[52] S. Dominguez-Medina, S. McDonough, P. Swanglap, C. F. Landes, and S. Link. (2012). "In Situ Measurement of Bovine Serum Albumin Interaction with Gold Nanospheres". *Langmuir.* **28** (24): 9131-9139. 10.1021/la3005213.

[53] Z. Wang, T. Yue, Y. Yuan, R. Cai, C. Niu, and C. Guo. (2013). "Kinetics of Adsorption of Bovine Serum Albumin on Magnetic Carboxymethyl Chitosan Nanoparticles". *International Journal of Biological Macromolecules.* **58** : 57-65. 10.1016/j.ijbiomac.2013.03.037.

[54] J. Lyklema. (1995). "Fundamentals of Interface and Colloid Science". Academic Press. 10.1016/S1874-5679(06)80004-8.

[55] Y. Yu, Y. Y. Zhuang, Z. H. Wang, and M. Q. Qiu. (2004). "Adsorption of Water-Soluble Dyes onto Modified Resin". *Chemosphere.* **54** (3): 425-430. 10.1016/S0045-6535(03)00654-4.

[56] L. Abarca-Cabrera, P. Fraga-Garcia, and S. Berensmeier. (2021). "Bio–Nano Interactions: Binding Proteins, Polysaccharides, Lipids, and Nucleic Acids onto Magnetic Nanoparticles". *Biomaterials Research.* **25** : 12. 10.1186/s40824-021-00212-y.

[57] M. Rahmayanti, S. J. Santosa, and Sutarno. (2016). "Comparative Study on the Adsorption of [AuCl4]- onto Salicylic Acid- and Gallic Acid-Modified Magnetite Particles". *Indonesian Journal of Chemistry.* **16** (3): 329-337. 10.22146/ijc.21150.

[58] N. M. Fedortsov, E. V. Budkevich, I. A. Evdokimov, S. A. Ryabtseva, and R. O. Budkevich. (2022). "Bovine Serum Albumin with Gallic Acid: Molecular Modeling and Physicochemical Profiling". *Foods and Raw Materials.* **10** (1): 163-170. 10.21603/2308-4057-2022-1-163-170.